Field modulation of Rydberg-state populations of NO studied by femtosecond time-resolved photoelectron imaging

Bingxing Wang,[1,2] Benkang Liu,[1,2] Yanqiu Wang,[1] and Li Wang[1,*]

[1]*State Key Laboratory of Molecular Reaction Dynamics, Dalian Institute of Chemical Physics, Dalian 116023, People's Republic of China*

[2]*Graduate School of the Chinese Academy of Sciences, Beijing 100049, People's Republic of China*

(Received 16 September 2009; published 28 April 2010)

Femtosecond time-resolved velocity map imaging combined with multiphoton ionization was applied to study the optical field modulation of NO Rydberg-state populations. The $A\,^2\Sigma^+(\upsilon = 2)$ state is populated by absorption of one 271-nm photon. Two peaks in the photoelectron kinetic energy spectra, centered at 0.82 and 2.35 eV, are caused by ionization from the $A\,^2\Sigma^+(\upsilon = 2)$ state by time-delayed one-color and two-color multiphoton ionization, respectively. In the overlap region of the pump and probe light, the $C\,^2\Pi(\upsilon = 4)$ state is populated by a $1 + 1'$ excitation. When the pump laser intensity is increased, other Rydberg states ($E\,^2\Sigma^+$, $F\,^2\Delta$, and $D\,^2\Sigma^+$) are moved into resonance by a laser-induced Stark shift. These states can be populated only within the temporal overlap region of the pump and probe light. When the intensity of the pump laser is higher than 2.9×10^{12} W/cm^2, Rydberg-valence coupling between the $A\,^2\Sigma^+(\upsilon = 2)$ and $B\,^2\Pi(\upsilon = 4)$ states may play a key role, resulting in photoelectrons with kinetic energy of 0.37 eV. The coupling strength increases with increasing pump laser intensity.

DOI: 10.1103/PhysRevA.81.043421 PACS number(s): 32.80.Rm, 33.80.Rv, 33.20.Xx, 33.20.Tp

I. INTRODUCTION

Femtosecond laser technology has been widely applied to the fields of physics and chemistry in methods such as time-resolved chemical reaction dynamics [1–3]. Interesting phenomena have been reported in past decades in an intense femtosecond laser field, including above-threshold ionization [4,5], the ac Stark shift [6,7], harmonic generation [5,8], coherent phenomena [9,10], and laser-induced continuum structure [11]. Recently, chemical reaction control has become a hot topic in femtochemistry [6,7,12–15].

The dynamics of NO in a femtosecond laser field have been extensively studied [13,16–22]. The ionization yields of different NO^+ electronic ground-state vibrational levels have been successfully controlled by feedback optimization of shaped ultrashort laser pulses [13]. Dynamic NO Stark effects have been comprehensively studied using fluorescence spectra and theoretical calculations [16–18]. Electronic states that were inaccessible by direct optical excitation were populated in an intense laser field. For example, the levels $\upsilon = 7$–10 of the $B\,^2\Pi$ state were populated by excitation from the ground electronic state to $\upsilon = 0$ of the $C\,^2\Pi$ state through *B*-*C* coupling [16]. It was suggested that coupling between the $A\,^2\Sigma^+$ and $B\,^2\Pi$ states was minor [16]. Dispersed fluorescence experiments on the $A\,^2\Sigma^+$ state in a femtosecond intense field showed that the vibrational levels of the $A\,^2\Sigma^+$ state might be mapped out of resonance as the laser intensity increased [17,18].

Recently, time-dependent photoelectron angular distributions from the $A\,^2\Sigma^+$ state ($\upsilon = 0$) have been measured by femtosecond photoelectron imaging [19]. The pump-laser wavelength was fixed at 226 nm (5.49 eV) to excite the (0,0) band of the *A*-*X* transition, while the probe-laser wavelength was varied from 255 nm (4.86 eV) to 323 nm (3.84 eV). The work focused on the time- and energy-dependent photoionization dynamics of the $A\,^2\Sigma^+(\upsilon = 0)$ state. The energy-dependent photoionization transition dipole moments were determined experimentally based on multichannel quantum defect theory.

Femtosecond time-resolved photoelectron spectroscopy (TRPES) has been applied to study the field modulation of populations in the $A\,^2\Sigma^+$, $B\,^2\Sigma^+$, and $C\,^2\Pi$ states via $2 + 1'$ multiphoton ionization [20]. The $C\,^2\Pi$ state ($\upsilon = 0$) was populated by the absorption of two 3.3-eV photons (380 nm) and ionized by a time-delayed 4.9-eV photon. The NO $A\,^2\Sigma^+(\upsilon = 3)$ state was populated by the coupling of the $A\,^2\Sigma^+$ and $C\,^2\Pi$ states by the ac Stark shift in the pump-laser field. Ionization from these two states produces photoelectrons with kinetic energies of 2.13 and 1.1 eV, respectively. The rapid modulation observed in the photoelectron spectra was assigned to the temporal perturbation of the Rydberg-valence interaction by the femtosecond pulse [20]. The Rydberg-valence coupling between the $B\,^2\Pi$ and $C\,^2\Pi$ states was highly sensitive to the pump pulse intensity, resulting in qualitatively different TRPES for the pump-dressed and the pump-prepared molecules. Photoelectrons with kinetic energies of 1.7 and 1.8 eV, observed in the overlapping region of the pump-probe pulses, were thought to be due to ionization from the mixed state. Photoelectrons with energies below 1 eV and between 1.1 and 1.7 eV were attributed to ionization from the Rydberg-valence mixed state [20].

The effects of the laser field on the potential curves of different NO electronic states have been well demonstrated theoretically [21,22]. Populations in the $A\,^2\Sigma^+$, $B\,^2\Sigma^+$, and $C\,^2\Pi$ states exhibited different time-dependent behaviors [21]. The coupling strength between the *B* and *C* states changed with the laser intensity, resulting in different TRPES at delay times of 0 and 400 fs [20]. The Rydberg-Rydberg Raman coupling and quantum interference between different pathways considerably influenced the peak intensities of the photoelectron kinetic energy spectra and the ionization probability of NO [22]. The population in the $D\,^2\Sigma^+$ state was

*Corresponding author: liwangye@dicp.ac.cn

partially transferred to the $M\,^2\Sigma^+$ state via Raman coupling. In the temporal overlap region, the populations of the $D\,^2\Sigma^+$ and $M\,^2\Sigma^+$ states oscillated with the delay time.

Few current studies focusing on the field modulation of NO electronic-state populations in a femtosecond two-color laser field have been reported [13,20]. While the field modulation of the $C\,^2\Pi$ state has been extensively studied, field effects on other electronic states, particularly the $A\,^2\Sigma^+$ state, have seldom been addressed. In this paper, we report our findings on the optical modulation of NO Rydberg-state populations using femtosecond time-resolved imaging methods combined with multiphoton ionization ionization. The kinetic energy and angular distributions can be obtained simultaneously; both are helpful in the assignment of photoelectrons from different electronic states. In Ref. [19], the $A\,^2\Sigma^+(\upsilon = 0)$ state, which was far from the potential crossing point ($\upsilon = 3$ in the $A\,^2\Sigma^+$ state), was populated. The authors of Ref. [20] addressed the $C^2\Pi(\upsilon = 0)$ state, which was degenerate with the $B\,^2\Pi(\upsilon = 7)$ valence state and slightly above the $A\,^2\Sigma^+(\upsilon = 3)$ state. In contrast to these earlier experiments, the $A\,^2\Sigma^+(\upsilon = 2)$ and $C\,^2\Pi(\upsilon = 4)$ states are addressed here. The $A\,^2\Sigma^+(\upsilon = 2)$ state, which is close to the $B\,^2\Pi(\upsilon = 4)$, and $D\,^2\Sigma^+(\upsilon = 0)$ states, is populated by two photons of the pump light. The $C\,^2\Pi$ state ($\upsilon = 4$), which is close to the $E\,^2\Sigma^+(\upsilon = 1)$ and $F\,^2\Delta(\upsilon = 0)$ states, is accessed by the absorption of one pump and one probe photon in the temporal overlap region. Because of the nature of this excitation, photoelectrons from these states can be observed only within the overlap region of the pump and probe light. As the pump laser intensity increases, populations in these states evidently change, resulting in relative intensity variations in TRPES. The $4s\,\sigma\ E\,^2\Sigma^+(\upsilon = 1)$ state is shifted out of resonance, and the $3d\,\delta\,F\,^2\Delta(\upsilon = 0)$ state is preferred as the pump intensities increase. Laser-induced Rydberg-valence mixing of the $A\,^2\Sigma^+(\upsilon = 2)$ and $B\,^2\Pi(\upsilon = 4)$ states results in the generation of photoelectrons with kinetic energies of 0.37 eV through a one-photon ionization pathway. The Rydberg-valence coupling between the $A\,^2\Sigma^+$ Rydberg state and the $B\,^2\Pi$ valence state may be important in two-photon resonance excitation within the femtosecond laser field.

II. EXPERIMENTAL SETUP

The experimental details of our laser system have been described elsewhere [23]. Briefly, our femtosecond laser is a home-built, solid-state, chirped-pulse amplified Ti:sapphire femtosecond laser comprised of a seed oscillator, an amplifier with a stretcher, and a compressor. The fundamental light is centered at 814 nm (with a 30-nm bandwidth, 70-fs pulse width, and 20-Hz repetition rate). After frequency doubling with a thin β-barium borate (BBO) crystal, the output is decomposed into two beams of 814 and 408 nm (the second harmonic with a 6-nm bandwidth) by a dichroic beam splitter. The 271-nm laser beam is generated (the third harmonic with about a 3-nm bandwidth) by sum-frequency mixing of these two beams in another BBO crystal. Subsequently, two beams of 408 nm (3.04 eV) and 271 nm (4.57 eV) are obtained from the output with another dichroic beam splitter. These beams serve as the pump and probe light, respectively. The probe beam is temporally delayed relative to the pump beam by a computer-controlled step-motor-driven linear translator (Sigma Koki, SGSP26-150). The two laser beams are focused by a fused silica lens with $f = 380$ and 450 mm, respectively, and then collinearly introduced into the vacuum chamber with a dichroic mirror. Both the beams are polarized such that they are parallel to the detector plane and perpendicular to the molecular beam. During experimentation, the peak intensity of the laser pulse at the intersection with the molecular beam is adjusted by moving the focal point of the lens.

The femtosecond time-resolved velocity map imaging setup [23] is similar to that designed by Eppink and Parker [24]. Briefly, it consists of a molecular-beam source chamber and an ionization-flight detection chamber. The detection chamber was kept below 5×10^{-6} Pa with the molecular beam on. Nitric oxide (5% in helium) was expanded into the source chamber through a pulsed nozzle (General Valve, with a 0.5-mm orifice) at a stagnation pressure of 1.2 atm. The supersonic molecular beam is collimated by a conical skimmer and intersects perpendicularly with the two laser beams in a two-stage ion lens region. Photoelectrons are extracted into a 40-cm field-free region, which is doubly shielded against stray magnetic fields by a μ-metal tube. At the end of the time-of-flight tube, the electrons strike a two-stage multichannel plate detector backed by a phosphor screen. The images on the screen are captured with a thermoelectrically cooled charge-coupled-device video camera (LAVISION Inc., Imager QE). Each photoelectron image is the integration of more than 10 000 laser shots. The emission from the phosphor screen is monitored by a photomultiplier connected to a 5 GS/s digital phosphor oscilloscope (Tektronix Inc., TDS3054B) GPIB interfaced with a computer. An inverse Abel transform is applied to calculate the slices through the three-dimensional (3D) scattering distributions of the photoelectrons from the observed 2D projection images.

III. RESULTS AND DISCUSSION

A. Photoelectron imaging of nitric oxide

Nitric oxide is one of the most studied diatomic molecules of recent decades. The optically accessible electronic states of both the neutral and cationic forms are well characterized [25]. The adiabatic ionization energy of NO (V_{ion}) is 9.2644 eV [20].

Photoelectron velocity mapping imaging is able to assess the photoelectron kinetic energy (E_{kin}) and angular distributions simultaneously. Figure 1 presents the raw images (upper part) as well as the corresponding inverse Abel transform slice images (lower part) obtained at different pump-probe delay times. Figure 1(a) shows images (raw and inversed) obtained using one-color irradiation (408 nm). The intensities of the pump and probe beams are estimated to be about 1.9×10^{12} and 5.7×10^{11} W/cm^2, respectively. Figure 2 illustrates the photoelectron kinetic energy distributions in Fig. 1. One-color multiphoton ionization (408 nm) produces only one peak, centered at 2.35 eV and marked as *a* in Fig. 2, which is attributed to a $2 + 2$ multiphoton ionization. The absorption of two 3.04-eV photons is in resonance with the $3s\,\sigma\ A\,^2\Sigma^+(\upsilon = 2)$ Rydberg state [25]. The absorption of another two 3.04-eV photons projects NO into the cationic

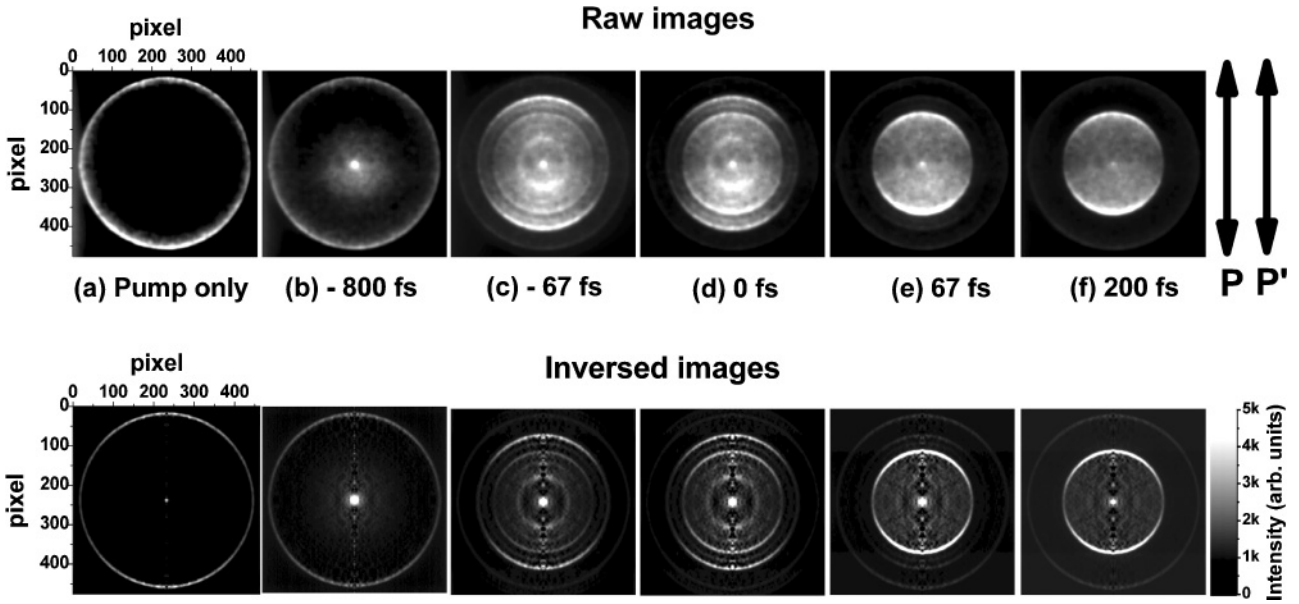

FIG. 1. Photoelectron images: raw (upper part) and inverse-Abel-transformed (lower part) images for the pump only and at different pump-probe delay times. The intensities of the pump and probe light are 1.9×10^{12} and 5.7×10^{11} W/cm^2, respectively. Arrows on the left side denote the polarization directions of pump and probe laser, respectively.

state. Because of the similarities in the potential curves of the NO^+ cation state and the neutral Rydberg state $A\,^2\Sigma^+$, NO^+ will be mostly populated in the $\upsilon = 2$ state. The vibrational propensity rule $\Delta\upsilon = 0$ holds in the ionization step. Similar observations have been reported using 405-nm femtosecond laser excitations [13]. No other peak can be detected while the pump comes before the probe pulse, as shown in Figs. 1 and 2 at a delay time of 800 fs, indicating that the 271-nm pump laser is too weak to induce one-color multiphoton ionization.

As shown in Fig. 2, one can easily find differences among these spectra. In the pump-probe overlap region (Fig. 2, from -67 to 67 fs), there are an additional five peaks centered at 0.24, 0.50, 0.82, 1.1, and 1.4 eV, labeled *f*, *e*, *b*, *c,* and *d*, respectively. Of these peaks, *f*, *e*, *c,* and *d* appear at the beginning of the overlap region and disappear after it. Only peak *b*, centered at 0.82 eV, exists when the pump-probe delay time is longer than 67 fs. This peak is attributed to the one-4.57-eV-photon ionization of $A\,^2\Sigma^+(\upsilon = 2)$, populated by the absorption of two 3.04-eV photons. The lifetimes of the $A\,^2\Sigma^+$ states with vibrational numbers $\upsilon < 3$ have been reported to be about 200 ns [26]. The lifetimes of the $D\,^2\Sigma^+$ states with vibrational numbers $\upsilon < 3$ were longer than 10 ns [27]. One 4.57-eV photon projects NO from the $A\,^2\Sigma^+(\upsilon = 2)$ state to the cationic state $X\,^1\Sigma^+(\upsilon = 2)$ owing to the propensity rule. The kinetic energies of peaks *a* and *b* are consistent with $2 + 2$ and $2 + 1'$ (or $1' + 2$) multiphoton ionization schedules, as defined in Eqs. (1) and (2), respectively.

$$E_{\text{kin}}^{\text{peak a}} = 2h\nu_{\text{pump}} + 2h\nu_{\text{probe}} - (V_{\text{ion}} + E_{iv} - E_{mv}), \quad (1)$$

$$E_{\text{kin}}^{\text{peak b}} = 2h\nu_{\text{pump}} + h\nu_{\text{probe}} - (V_{\text{ion}} + E_{iv} - E_{mv}). \quad (2)$$

E_{mv} and E_{iv} denote vibrational levels of the intermediate Rydberg and cationic states, respectively. The anisotropy parameters (β) of these two peaks at a 3.2-ps delay time are similar, 1.2 and 1.3, respectively. This similarity also confirms that peaks *a* and *b* result from the ionization of the same Rydberg state, $A\,^2\Sigma^+$.

Considering the laser pulse width, we prefer to assign the other four peaks to one-3.04-eV-photon ionization of some intermediate states that are populated by the coexcitation of one 4.57- and one 3.04-eV photon. Naturally, such an

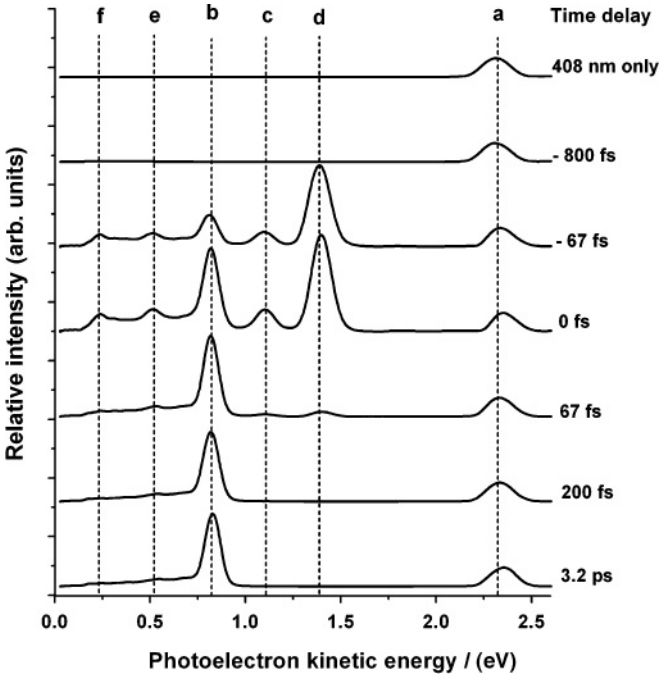

FIG. 2. Photoelectron kinetic energy (PKE) distributions with the pump only and at different delay times (-800, -67, 0, 67, and 200 fs and 3.2 ps). Experimental conditions are same as in Fig. 1.

TABLE I. Assignments of the observed photoelectrons. Photoelectron kinetic energies (E_{kin}) are derived from Fig. 2. The energies of Rydberg states (T) and the quantum defect (δ) are calculated from Eq. (1). The anisotropy parameters (β) are extracted from the image at 0 fs pump-probe delay time.

	Peak a	Peak b	Peak c	Peak d	Peak e	Peak f
E_{kin} (eV)	2.35	0.82	1.1	1.4	0.50	0.24
Ionization	$2+2$	$2+1'$	$1'+1+1$	$1'+1+1$	$1'+1+1$	$1'+1+1$
T (eV)	5.53	5.53	7.32	7.62	6.75	6.51
	(5.45)[a]	(5.45)[a]	(7.52)[a]	(7.66)[a]	(6.58)[a]	(6.45)[a]
State	$3s\,\sigma\,A\,^2\Sigma^+$	$3s\,\sigma\,A\,^2\Sigma^+$	$4s\,\sigma\,E\,^2\Sigma^+$	$3d\,\delta\,F\,^2\Delta$	$3p\,\sigma\,D\,^2\Sigma^+$	$3p\,\pi\,C\,^2\Pi$
δ	1.10	1.10	1.35	0.12	0.69	0.80
	(0.98)[b](1.10)[c]	(0.98)[b](1.10)[c]	(0.98)[b]	(0.08)[b]	(0.69)[b](0.74)[c]	(0.75)[b]
β	2.0	1. 08	1.5	1.9	0.5	0.4

[a]From Ref. [25].
[b]From Ref. [28].
[c]From Ref. [29].

excitation exists only in the pump-probe overlap area of the cross-correlation region.

Optically accessible electronic states of 408 or 271 nm show Rydberg-state characteristics [25]. These states should have long lifetimes: 40 ns for $4s\,\sigma\,E\,^2\Sigma^+(\upsilon=0)$ and 27 ns for $3d\,\delta\,F\,^2\Delta(\upsilon=0)$ [27]. Such long lifetimes are inconsistent with our observation in Fig. 2. These four peaks can only be observed in the pump-probe overlap region. Considering the bandwidth of the femtosecond pulses, the total energy of one 4.57 and one 3.04 photon, $(1+1')$, ranges from 7.5 to 7.7 eV with a center at 7.6 eV. The energy gap in the NO^+ ground-state vibrational states is about 290 meV. In a supersonic molecular beam NO stays mainly in the electronic ground state with $\upsilon=0$ (0.13 eV) [20]. Ionization from the ground state ($\upsilon=0$) via a $1'+2$ multiphoton ionization will generate photoelectrons with excess energy. The excess energies at the vibrational levels of the ion ground state are 1.40 ($\upsilon=0$), 1.1 ($\upsilon=1$), 0.81 ($\upsilon=2$), 0.51 ($\upsilon=3$), and 0.22 eV ($\upsilon=4$), respectively. Because of the limitations of the propensity rule, intermediate states with corresponding vibrational numbers should be populated by one 4.57-eV photon or a $1'+1$ excitation. The states accessible by a $1+1'$ excitation are $3p\,\pi\,C\,^2\Pi(\upsilon=4)$, $3p\,\sigma D\,^2\Sigma^+(\upsilon=3)$, $4s\,\sigma\,E\,^2\Sigma^+(\upsilon=1)$, and $3d\,\delta\,F\,^2\Delta(\upsilon=0)$. These states are almost degenerate with the $3p\,\pi\,C\,^2\Pi(\upsilon=4)$ state, which can be directly populated by a $1+1'$ excitation. For example, $4s\,\sigma\,E\,^2\Sigma^+(\upsilon=1)$ and $3d\,\delta\,F\,^2\Delta(\upsilon=0)$ are only 60 and 50 meV above the $3p\,\pi\,C\,^2\Pi(\upsilon=4)$ state, respectively. These states are easily moved into resonance by intense external-field-induced Stark shifts followed by one-photon ionizations. Because of the nature of the coexcitation, these states can survive only in the overlap region of the pump-probe light. Morse potential functions were applied to calculate the potential curves of different electronic states, as in Refs. [16,20–22]. The anharmonicity constants of the Morse functions for different electronic states and vibrational energies are taken from Ref. [25].

The kinetic energies of the photoelectrons from these states resulting from one-3.04-eV-photon ionization are 0.24 eV [peak f, from $3p\,\pi\,C\,^2\Pi(\upsilon=4)$], 0.50 eV [peak e, from $3p\,\sigma\,D\,^2\Sigma^+(\upsilon=3)$], 1.1 eV [peak c, from $4s\,\sigma\,E\,^2\Sigma^+(\upsilon=1)$], and 1.4 eV [peak d, from $3d\,\delta\,F\,^2\Delta(\upsilon=0)$, respectively. The anisotropy parameters (β) of these four peaks at a delay time of zero are also listed in Table I. The energies of the zero vibrational levels, T(Rydberg), in resonance can be easily deduced from the following formula:

$$E_{kin} = T(\text{Rydberg}) + h\upsilon - V_{ion} = h\upsilon - \frac{R}{(n-\delta)^2}, \quad (3)$$

where υ is the laser frequency, V_{ion} is the adiabatic ionization energy, R is the Rydberg constant, n is the principal quantum number, and δ is the quantum defect.

The energies of these Rydberg states and their corresponding quantum defects are listed in Table I; they are consistent with reported values [25,28,29]. The values of $\delta=1.10$–1.35 confirm that photoelectrons with 0.82 and 1.10 eV (peaks b and c) originate from the $3s\,\sigma\,A\,^2\Sigma^+$ and $4s\,\sigma\,E\,^2\Sigma^+$ Rydberg states, respectively. The $3p\,\sigma\,D\,^2\Sigma^+$ Rydberg state has a small quantum defect, peak e, as shown in Table I. The quantum defects of the $3s\,\sigma\,A\,^2\Sigma^+$ and $3p\,\sigma\,D\,^2\Sigma^+$ states have been recently calculated to be 1.10 and 0.74, respectively [29]. The value $\delta=0.12$ for peak d verifies that photoelectrons with energy 1.40 eV are from the $3d\,\delta\,F\,^2\Delta$ Rydberg state. The anisotropy parameters of these peaks were also determined and are listed in Table I. The angular distribution of photoelectrons from an s Rydberg state shows more anisotropy than that from a p Rydberg state [30]. Both the quantum defects and anisotropy parameters of photoelectrons of different energies support our assignments.

B. Coupling between the $A\,^2\Sigma^+$ and $B\,^2\Pi$ states

As the pump laser intensity increases, the ratio of peak b to peak a decreases, as illustrated in Fig. 3. As the pump laser becomes more intense, NO in the $A\,^2\Sigma^+$ state can be ionized by the absorption of another two 3.04-eV photons (peak a), which decreases the population of the $A\,^2\Sigma^+$ state. This decrease leads to the weaker signal intensity of peak b with time-delayed probe light.

As the 408-nm laser increases from 1.9×10^{12} to 23×10^{12} W/cm^2, peak d shifts to a slightly higher energy, from 1.40 to 1.43 eV, while the other peaks remain at their original positions. The relative intensity of peak c decreases in the stronger 408-nm laser field. As assigned in Table I, peaks c and d come from one-3.04-eV-photon ionizations of the

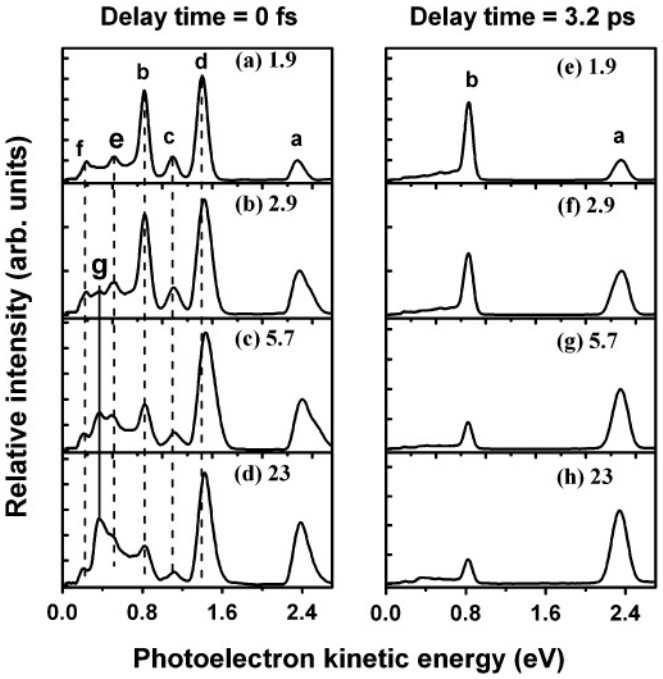

FIG. 3. Photoelectron kinetic energy distributions at different pump intensities. The pump intensities ($\times 10^{12}$ W/cm^2) are 1.9 [(a) and (e)], 2.9 [(b) and (f)], 5.7 [(c) and (g)], and 23 [(d) and (h)], respectively. The probe intensity is kept at 5.7 $\times$ 10^{11} W/cm^2. The left panel is at pump-probe delay time of zero, the right panel at 3.2 ps.

$4s\,\sigma\, E\,^2\Sigma^+(\upsilon = 1)$ and $3d\,\delta\, F\,^2\Delta(\upsilon = 0)$ states, respectively. As the 408-nm laser intensity increases, these two states increase their energies, resulting in the $4s\,\sigma\, E\,^2\Sigma^+(\upsilon = 1)$ state stepping out of resonance (intensity decrease of peak *c*).

Another peak, positioned at 0.37 eV and marked as *g* in Fig. 3, emerges as the pump laser intensity becomes stronger than 2.9 $\times$ 10^{12} W/cm^2. Peak *g* becomes stronger than peak *b* and comparable to peak *a* when the laser intensity is about 23 $\times$ 10^{12} W/cm^2. Photoelectrons with energies of 0.37 eV were not reported in Refs. [19] and [20]. The ponderomotive shifts are about 30, 45, 89, and 357 meV, corresponding respectively to the pump intensities 1.9 $\times$ 10^{12}, 2.9 $\times$ 10^{12}, 5.7 $\times$ 10^{12}, and 23 $\times$ 10^{12} W/cm^2 in Fig. 3. The Stark shift of bound states ($A\,^2\Sigma^+$, for example) is expected to be much smaller (0.36 eV) at an intensity of 60 $\times$ 10^{12} W/cm^2 at 400 nm [17]. Peak *g*, however, cannot be understood in the context of the Stark shift effect. We noticed that the position of peak *g* remains unchanged while its intensity grows quickly as the 408-nm laser intensity increases. As pointed out by Ludowise *et al.* [20], this experimental observation implies that photoelectrons with energies of 0.37 eV have some partial valence character.

A possible way to generate photoelectrons with 0.37 eV energy is through coupling between the $A\,^2\Sigma^+$ and $B\,^2\Pi$ states. The $B\,^2\Pi(\upsilon = 4)$ state is degenerate with the $A\,^2\Sigma^+(\upsilon = 2)$ state. This degeneracy may cause mixing between these two levels in an intense external field, resulting in possible ionization from the $B\,^2\Pi(\upsilon)$ to the cationic state of the same vibrational number. Although direct, one-electron ionization from the pure $B\,^2\Pi$ state to the cationic ground state is forbidden, one-photon ionization from the mixed $B\,^2\Pi$–$A\,^2\Sigma^+$ Rydberg state is possible [20,31]. Large optical Stark shifts have been observed in the two-photon transition spectrum of NO from the ground state to the $A\,^2\Sigma^+$ state [32]. It has been suggested that the $A\,^2\Sigma^+$ state is perturbed by interactions with close lying electronic states coupled to the laser field. The strongest perturbation of the $A\,^2\Sigma^+$ state came from the $B\,^2\Pi$ vibrational level [32]. Simulation spectra that included the coupling effect between the $A\,^2\Sigma^+$ and $B\,^2\Pi$ states fit well with the asymmetric broadening in the two-photon excitation spectra of the $X\,^2\Pi(\upsilon = 0) \rightarrow A\,^2\Sigma(\upsilon = 0)$ transition [32]. Theoretical calculations also suggested that the $A\,^2\Sigma^+$ state could be weakly coupled to the $B\,^2\Pi$ state, resulting in a series of well-defined peaks corresponding to the Stark shifts of vibrational levels in and out of resonance with the increasing pump laser intensity [16]. Time-resolved NO fluorescence experiments in the $A\,^2\Sigma^+(\upsilon = 2)$ state and related theoretical calculations [18] also suggested that the intensity reduction in the $A\,^2\Sigma^+ \rightarrow X\,^2\Pi$ fluorescence was due to the additional coupling of the $B\,^2\Pi$ valence state. The dependence of the ac Stark shift on the properties of the potential surfaces could modify the weak coupling between the $A\,^2\Sigma^+(\upsilon = 2)$ and valence $b\,^4\Sigma^-(\upsilon = 2)$ states, contributing to the control over the vibrational products of NO^+ [13]. Based on these previous reports, we suppose that photoelectrons with an energy of 0.37 eV result from ionization of the $B\,^2\Pi(\upsilon = 4)$ state, which is populated through coupling with the $A\,^2\Sigma^+(\upsilon = 2)$ state in the presence of an intense pump laser field. At long delay times without the pump laser field, the population in the $B\,^2\Pi$ valence state cannot be ionized to the cationic ground state.

More ionization channels are observed in our experiments than in previous reports [19,20]. The main difference in the results is that we are addressing the $A\,^2\Sigma^+(\upsilon = 2)$ and $C\,^2\Pi(\upsilon = 4)$ states, which are close to the electronic states involved, as we noted previously. These almost degenerate

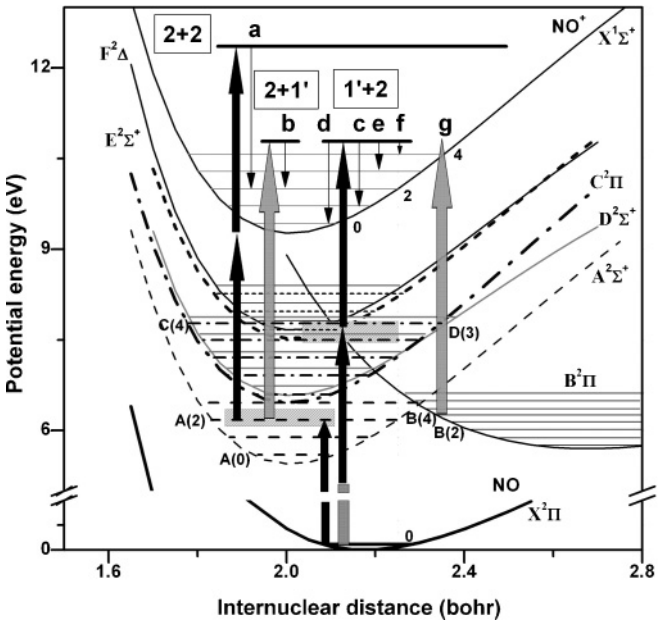

FIG. 4. Possible ionization pathways of NO observed in the present experiment. The 408-nm pathway is represented by the solid arrow and the 271-nm one by the gray arrow.

states are moved into resonance by either Stark shifts or coupling induced by an intense external field. The electronic states involved in our experiments and the corresponding Morse potential curves are illustrated in Fig. 4. The thin, solid arrowed lines in Fig. 4, denoted *a*–*g*, correspond to different ionization channels, while the lengths of the arrowed lines represent the corresponding excess energies in eV. The populated states in previous reports, $A\,^2\Sigma^+(\upsilon = 0)$ in Ref. [19], and $C\,^2\Pi(\upsilon = 0)$, $A\,^2\Sigma^+(\upsilon = 3)$, and $B\,^2\Pi(\upsilon = 7)$ in Ref. [20], are far from the states involved in our experiment.

IV. CONCLUSIONS

In this paper, femtosecond time-resolved imaging with multiphoton ionization was used to examine the optical modulation of the electronic state populations of nitric oxide. Photoelectron kinetic energy distributions and angular distributions indicate that intra-Rydberg coupling and Rydberg-valance coupling contribute to the spectra at a delay time of zero. As the pump and probe pulses overlap, ionization from the Rydberg states $4s\,\sigma\,E\,^2\Sigma^+$, $3d\,\delta\,F\,^2\Delta$, $3p\,\sigma\,D\,^2\Sigma^+$, and $3p\,\pi\,C\,^2\Pi$, populated by the absorption of one 4.57-eV photon and one 3.04-eV photon, projects photoelectrons with different excess kinetic energies. Because of the nature of this excitation, photoelectrons generated from these states can be observed only within the overlap region of the pump and probe light. As the pump laser intensity increases, populations in these states evidently change, resulting in relative intensity variations of photoelectrons with different kinetic energies. The $4s\,\sigma\,E\,^2\Sigma^+(\upsilon = 1)$ state is shifted out of resonance and the $3d\,\delta\,F\,^2\Delta(\upsilon = 0)$ state becomes preferred as the pump intensities increase. Photoelectrons with a kinetic energy of 0.37 eV in the pump-probe overlap region result from ionization of the Rydberg-valence mixture of the $A\,^2\Sigma^+(\upsilon = 2)$ and $B\,^2\Pi(\upsilon = 4)$ states. As the pump laser becomes intense enough ($>2.9 \times 10^{12}$ W/cm^2), the $B\,^2\Pi(\upsilon = 4)$ state becomes optically reachable through coupling with the $A\,^2\Sigma^+$ state. Our results indicate that this coupling strength increases with the pump laser intensity.

ACKNOWLEDGMENTS

This work is supported by the National Natural Science Foundation of China (Grant Nos. 20633070 and 20473090).

[1] J. C. Polanyi and A. H. Zewail, Acc. Chem. Res. **28**, 119 (1995).
[2] M. Dantus and A. Zewail, Chem. Rev. **104**, 1717 (2004).
[3] R. E. Carley, E. Heesel, and H. H. Fielding, Chem. Soc. Rev. **34**, 949 (2005).
[4] M. Busuladzic, A. Gazibegovic-Busuladzic, D. B. Milosevic, and W. Becker, Phys. Rev. Lett. **100**, 203003 (2008).
[5] C. P. Liu, T. Nakajima, T. Sakka, and H. Ohgaki, Phys. Rev. A **77**, 043411 (2008).
[6] R. J. Levis, G. M. Menkir, and H. Rabitz, Science **292**, 709 (2001).
[7] B. J. Sussman, D. Townsend, M. Y. Ivanov, and A. Stolow, Science **314**, 278 (2006).
[8] P. Tzankov, O. Steinkellner, J. A. Zheng, M. Mero, W. Freyer, A. Husakou, I. Babushkin, J. Herrmann, and F. Noack, Opt. Express **15**, 6389 (2007).
[9] J. K. L. Knappenberger, E. B. W. Lerch, P. Wen, and S. R. Leone, J. Chem. Phys. **125**, 174314 (2006).
[10] P. Tian, D. Keusters, Y. Suzaki, and W. S. Warren, Science **300**, 1553 (2003).
[11] O. Faucher, E. Hertz, B. Lavorel, R. Chaux, T. Dreier, H. Berger, and D. Charalambidis, J. Phys. B **32**, 4485 (1999).
[12] T. P. Rakitzis, A. J. van den Brom, and M. H. M. Janssen, Science **303**, 1852 (2004).
[13] E. Hertz, G. Nersisyan, N. A. Papadogiannis, and D. Charalambidis, J. Chem. Phys. **118**, 595 (2003).
[14] H. Rabitz, R. de Vivie-Riedle, M. Motzkus, and K. Kompa, Science **288**, 824 (2000).
[15] M. Wollenhaupt, V. Engel, and T. Baumert, Annu. Rev. Phys. Chem. **56**, 25 (2005).
[16] T. Dove, T. W. Schmidt, R. B. Lopez-Martens, and G. Roberts, Chem. Phys. **267**, 115 (2001).
[17] R. B. Lopez-Martens, T. W. Schmidt, and G. Roberts, Phys. Rev. A **62**, 013414 (2000).
[18] T. W. Schmidt, R. B. Lopez-Martens, and G. Roberts, J. Phys. B **37**, 1125 (2004).
[19] M. Tsubouchi and T. Suzuki, J. Chem. Phys. **121**, 8846 (2004).
[20] P. Ludowise, M. Blackwell, and Y. Chen, Chem. Phys. Lett. **258**, 530 (1996).
[21] Q. T. Meng, G. H. Yang, H. L. Sun, K. L. Han, and N. Q. Lou, Phys. Rev. A **67**, 063202 (2003).
[22] S. M. Wang, S. L. Cong, K. J. Yuan, and Y. Y. Niu, Chem. Phys. Lett. **417**, 164 (2006).
[23] W. Guo, J. Zhu, B. Wang, Y. Wang, and L. Wang, Phys. Rev. A **77**, 033415 (2008).
[24] A. T. J. B. Eppink and D. H. Parker, Rev. Sci. Instrum. **68**, 3477 (1997).
[25] K. P. Huber and G. Herzberg, *Constants of Diatomic Molecules* (Van Nostrand Reinhold Co., New York, NY, 1979).
[26] T. B. Settersten, B. D. Patterson, and J. A. Gray, J. Chem. Phys. **124**, 234308 (2006).
[27] J. Luque and D. R. Crosley, J. Chem. Phys. **112**, 9411 (2000).
[28] E. Lindholm, Ark. Fys. **40**, 97 (1969).
[29] A. M. Velasco, E. Bustos, I. Martín, and C. Lavín, Int. J. Quantum Chem. **99**, 511 (2004).
[30] J. Cooper and R. N. Zare, J. Chem. Phys. **48**, 942 (1968).
[31] M. G. White, M. Seaver, W. A. Chupka, and S. D. Colson, Phys. Rev. Lett. **49**, 28 (1982).
[32] W. M. Huo, K. P. Gross, and R. L. McKenzie, Phys. Rev. Lett. **54**, 1012 (1985).